Mitochondrial uncouplers impair human sperm motility without altering ATP content

Short Title: Mitochondrial uncouplers reduce human sperm motility but not ATP content

Will M. Skinner[1], Natalie T. Petersen[2,#3], Bret Unger[4], Shaogeng Tang[5,6], Emiliano Tabarsi[2,#7], Julianna Lamm[2,#8], Liza Jalalian[9], James Smith[10], Ambre M. Bertholet[11,#12], Ke Xu[4,13,14], Yuriy Kirichok[11], Polina V. Lishko[2,15,*].

[1] Endocrinology Graduate Group, University of California, Berkeley, Berkeley, California, United States of America

[2] Department of Molecular and Cell Biology, University of California, Berkeley, Berkeley, California, United States of America

[3] Department of Obstetrics and Gynecology, Stanford University School of Medicine, Palo Alto, California, United States of America

[4] Department of Chemistry, University of California, Berkeley, Berkeley, California, United States of America

[5] Department of Biochemistry, Stanford University School of Medicine, Stanford, California, United States of America

[6] Sarafan ChEM-H, Stanford University, Stanford, California, United States of America

[7] Keck School of Medicine, University of Southern California, Los Angeles, California, United States of America

[8] Dewpoint Therapeutics, Boston, Massachusetts, United States of America

[9] Department of Obstetrics and Gynecology, University of California, San Francisco Center for Reproductive Health, San Francisco, California, United States of America

[10] Department of Urology, University of California, San Francisco, San Francisco, California, United States of America

[11] Department of Physiology, University of California San Francisco, San Francisco, California, United States of America

[12] Department of Physiology, David Geffen School of Medicine, University of California Los Angeles, Los Angeles, California, United States of America

[13] California Institute for Quantitative Biosciences, University of California, Berkeley, California, United States of America

[14] Chan Zuckerberg Biohub, San Francisco, California, United States of America

[15] Center for Reproductive Longevity and Equality, Buck Institute for Research on Aging, Novato, California, United States of America

*Corresponding Author: Polina V. Lishko

Email: lishko@berkeley.edu

Author Contributions: W.M.S. and P.V.L conceived the project and designed experiments. W.M.S. conducted most experiments and analyzed most data, except as noted below, and wrote the manuscript. N.T.P. and W.M.S. performed *in vitro* fertilization experiments. B.U. and W.M.S. conducted STORM and B.U. analyzed data, under supervision of K.X. S.T. produced Izumo1 antibodies used during acrosome reaction assays. E.T. and J.L. assisted with multiple experiments. L.J. and J.S. enabled access to and training on computer-aided sperm analysis machines for motility assays performed by W.M.S. A.M.B. performed mitochondrial patch-clamp experiments and analyzed that data, under supervision of Y.K. P.V.L and W.M.S. performed human sperm patch-clamp electrophysiology. All of the authors discussed the results and commented on the manuscript.

Conceptualization: W.M.S and P.V.L

Data Curation: W.M.S.

Formal Analysis: W.M.S. and A.M.B.

Funding Acquisition: P.V.L. and W.M.S.

Investigation: W.M.S., N.T.P., B.U., E.T., J.L., A.M.B., P.V.L

Methodology: W.M.S., B.U., A.M.B, P.V.L

Project Administration: W.M.S.

Resources: W.M.S., S.T., L.J., J.S., K.X., Y.K., P.V.L.

Supervision: J.S., K.X., Y.K., P.V.L.

Validation: W.M.S.

Visualization: W.M.S., B.U., A.M.B

Writing – Original Draft Preparation: W.M.S.

Writing – Review & Editing: All Authors

Competing Interest Statement: W.M.S., P.V.L, E.T., A.M.B., and Y.K are co-inventors on a patent related to this work, which UC Berkeley has licensed to YourChoice Therapeutics, for which P.V.L is a co-founder, and Y.K. is a shareholder. The other authors declare no competing interests.

Abbreviations:

ANT: Adenine nucleotide translocase
ALH: Amplitude of lateral head displacement
ATP: Adenosine triphosphate
AUC: Area under the curve
BAM15: (N5,N6-bis(2-Fluorophenyl)-[1,2,5]oxadiazolo[3,4-b]pyrazine-5,6-diamine**)**
BAPTA: (1,2-bis(o-aminophenoxy)ethane-N,N,N′,N′-tetraacetic acid)
BSA: Bovine serum albumin
CATR**:** Carboxyatractyloside
COXIV: Cytochrome c oxidase subunit 4 isoform 1, mitochondrial
DNP: 2, 4, Dinitrophenol
EGTA: (ethylene glycol-bis(β-aminoethyl ether)-N,N,N′,N′-tetraacetic acid)
FCCP: Trifluoromethoxyphenylhydrazone
FDA: Food and Drug Administration
HEPES: (4-(2-hydroxyethyl)-1-piperazineethanesulfonic acid)
HRP: Horseradish peroxidase
HS: High Saline
HTF: Human Tubal Fluid
ICC: Immunocytochemistry
IMM: Inner mitochondrial membrane
KSOM: Potassium-supplemented simplex optimized medium
LIN: Linearity
MES: 2-(N-morpholino)ethanesulfonate.
MMP: Mitochondrial membrane potential
NEN: Niclosamide Ethanolamine
NMDG: N-methyl-D-glucamine
PI: propidium iodide
PMT: Photomultiplier tube
PVDF: polyvinylidene difluoride
STORM: Stochastic optical reconstruction microscopy
Tris: tris(hydroxymethyl)aminomethane
VCL: Curvilinear velocity

Abstract

Sperm motility is necessary for successful fertilization, but there remains controversy about whether human sperm motility is primarily powered by glycolysis or oxidative phosphorylation. To evaluate the plausibility of reducing human sperm mitochondrial ATP production as an avenue for contraceptive development, we treated human sperm with small-molecule mitochondrial uncouplers, which reduce mitochondrial membrane potential by inducing passive proton flow, and evaluated the effects on a variety of physiological processes that are critical for fertilization. We also sought to clarify the subcellular localization of Adenosine Nucleotide Translocator 4 (ANT4), a gamete-specific protein that has been suggested as a contraceptive target. We determined that ANT4 is mitochondrially localized, that induced mitochondrial uncoupling can be partially mediated by the ANT family, and that two uncouplers, Niclosamide Ethanolamine and BAM15, significantly decreased sperm progressive motility. However, these uncouplers did not reduce sperm ATP content or impair other physiological processes, implying that human sperm can rely on glycolysis for ATP production in the absence of functional mitochondria. Thus, since certain mitochondrial uncouplers impair motility through ATP-independent mechanisms, they could be useful ingredients in on-demand, vaginally-applied contraceptives. However, systemically delivered contraceptives that target sperm mitochondria to reduce their ATP production would need to be paired with sperm-specific glycolysis inhibitors.

118 **Main Text**

119

120 **Introduction**

121

122 Human sperm make one of the most remarkable and challenging journeys of any cell in
123 the human body. To reach the egg, the mature sperm must traverse a distance thousands of
124 times greater than their cell length, while surviving environments that differ greatly in viscosity,
125 pH, and oxygen and sugar concentrations (1,2). This journey requires vigorous flagellar motility
126 (3), and later asymmetrical "hyperactivated" flagellar bending (4), both of which require large
127 amounts of ATP. However, each human sperm possesses less than a fifty mitochondria (5), less
128 than almost any other metabolically active cell. Therefore, there has been persistent debate
129 about the role of mitochondria and oxidative phosphorylation in sperm physiology, with
130 metabolic studies showing that glycolysis is sufficient for human sperm ATP production (6), but
131 physiological and clinical studies showing that proper mitochondrial functionality is correlated
132 with high fertility in humans (7–10). Additionally, sperm contain many unique proteins and
133 protein isoforms, including metabolic enzymes (11), membrane transporters (12,13) and
134 receptors (14), and structural proteins (15). Many of these unique proteins have been appealing
135 targets for development of contraceptives that could disrupt sperm bioenergetics.

136 One of these unique transporter isoforms is Adenosine Nucleotide Translocator 4
137 (ANT4), which is gamete-specific (16) and required for spermatogenesis (17), but has an unclear
138 role in mature human sperm cells. Since its discovery, ANT4 has been seen as an attractive
139 candidate for the development of a male contraceptive (17–20). Efforts have been made to
140 develop specific ANT4 inhibitors, which were only able to achieve modest specificity (19,20).
141 Somatic ANT isoforms (ANT1, 2, and 3 in humans) are essential for transporting ATP and ADP

142 across the inner mitochondrial membrane (IMM) and have recently been found to be
143 responsible for mediating mild mitochondrial proton leak (or mitochondrial "uncoupling") across
144 the IMM in somatic, non-thermogenic tissues (21). It is also possible to activate ANT-mediated
145 proton leak using exogenous small molecule uncouplers (22). Therefore, we hypothesized that
146 instead of developing specific ANT4 inhibitors, it may be possible to develop novel small
147 molecule uncoupler contraceptives that act by specifically activating proton leak through ANT4,
148 thereby decreasing sperm mitochondrial membrane potential (MMP), ATP production, and
149 ultimately functionality. To pursue this hypothesis, we first needed to validate the idea that
150 breakdown of sperm MMP leads to functional dysregulations that could impair fertility. To do
151 so, we began by testing the physiological effects of various small molecule uncouplers on human
152 sperm cells.

153

154 **Results**

155

156 **Representative small molecule uncouplers decrease human sperm mitochondrial membrane**
157 **potential and impair basal motility.**

158 Four representative small molecule uncouplers were chosen to assess the effects of this
159 class of compounds on human sperm physiology: 2, 4, Dinitrophenol (DNP); carbonyl cyanide p-
160 trifluoromethoxyphenylhydrazone (FCCP); BAM 15 (N5,N6-bis(2-Fluorophenyl)-
161 [1,2,5]oxadiazolo[3,4-b]pyrazine-5,6-diamine**)**; and Niclosamide Ethanolamine (NEN) (Fig. 1A).
162 Live human sperm cells were treated with varying concentrations of each compound for 30
163 minutes at 37°C in noncapacitating media at pH 7.4, after which cells were stained with
164 MitoTracker Red CMX-Ros and mitochondrial membrane potential (MMP) was qualitatively

165 assessed using flow cytometry (Fig. 1B) and fluorescence microscopy (Fig. 1D). FCCP, BAM15,
166 and NEN were all able to dose-dependently reduce midpiece fluorescence and therefore MMP,
167 while DNP was unable to reduce midpiece fluorescence at concentrations up to 300 µM at this
168 pH level (Fig. S1A). The DMSO and Ethanol vehicles with which compounds were delivered did
169 not have a significant effect on mitochondrial fluorescence (Fig. S1A) and none of the
170 compounds decreased sperm viability (Fig. S1D). NEN and BAM15 reduced midpiece
171 fluorescence values more strongly than FCCP, had lower IC_{50} values, and are known to have
172 more favorable toxicity profiles (23,24), and so further experiments focused on these two
173 compounds.

174

175 **Figure 1: Representative small-molecule uncouplers dose-dependently reduce sperm**
176 **mitochondrial membrane potential and basal motility. A)** Chemical structures of representative
177 small molecule uncouplers used. **B)** Effects of SMUs on human sperm mitochondrial potential as
178 measured by MitoTracker Red fluorescence, normalized to average fluorescence of relevant
179 vehicle. Nonlinear least squares regression performed using an unweighted [inhibitor] vs.
180 response three parameter model (Hill Slope = -1.0), identifying "unstable" fits. Shaded areas
181 indicate 95% confidence bands for true location of each nonlinear fit curve. The nonlinear
182 regression fit had an Adjusted R^2 value of .8409 for NEN, .8179 for BAM15, and .7143 for FCCP.
183 Adjusted R^2 value for DNP was less than .1 and so curve is not shown or reported. Asymmetrical
184 95% CI intervals of IC_{50} for NEN: 1.415 µM to 5.380 µM; BAM15: 3.827 µM to 17.03 µM; FCCP:
185 9.148 µM to 64.05 µM**. C)** Model showing the possible mechanisms of action of small molecule
186 uncouplers in the sperm mitochondria and plasma membrane. **D)** Representative fluorescence
187 micrographs of sperm cells treated with MitoTracker Red CMX-Ros in the absence (top) and

188 presence (bottom) of 1 μM NEN. **E)** Effects of SMU on human sperm progressive motility as
189 measured by Computer-Aided Sperm Analysis. Data points represent the average of ≥500 sperm
190 cells. Nonlinear least squares regression performed and displayed as in B. The nonlinear
191 regression fit had an Adjusted R^2 value of .6323 for NEN, .2722 for BAM15, and <.1 for DMSO.
192 Asymmetrical 95% CI interval for NEN: 0.08256 μM to 0.6284 μM. Asymmetrical 95% CI interval
193 for BAM15: 0.1264 μM to 78.30 μM. **F)** Area Under the Curve quantification for graph E. Error
194 bars represent SEM, and each data point represents the area under the curve for all
195 concentrations of one biological replicate. Statistical significance calculated using Dunnett's
196 multiple comparisons test.
197
198 Next, we assessed the effects of NEN and BAM15 on human sperm motility, using
199 computer-aided sperm analysis (CASA). Both NEN and BAM15 reduced the percent of sperm
200 showing progressive motility (Fig. 1E,F) and NEN reduced the average curvilinear velocity (Fig.
201 S2A); NEN reduced sperm progressive motility percent below the 5th percentile of fertile men
202 (25) and showed a sub-micromolar IC_{50}.

203 **Adenosine Nucleotide Translocators (ANTs) partially mediate NEN-induced mitochondrial**
204 **uncoupling, and ANT4 is localized to the human sperm mitochondria**

205 In somatic, non-thermogenic tissues of the body, Adenosine Nucleotide Translocator
206 (ANT) proteins are known to mediate mild mitochondrial uncoupling under physiological
207 conditions and in the presence of exogenous uncouplers by inducing H^+ influx across the inner
208 mitochondrial membrane (21,22). Since sperm cells possess a unique isoform of the family
209 known as ANT4 (26), we investigated whether NEN-induced uncoupling is also mediated by the
210 ANT family of proteins. To do this, we performed mitochondrial patch-clamp electrophysiology,

211 through which it is possible to directly measure current across the inner mitochondrial
212 membrane. Indeed, in mouse heart mitochondria, which abundantly express ANT1 (27), 500 nM
213 NEN induced a strong inward H^+ current at physiological pH and negative voltage. This H^+
214 current was significantly reduced both in the presence of 1 µM Carboxyatractyloside (CATR), a
215 known ANT inhibitor (Fig. 2B, C), and in heart mitochondria from ANT1-knockout mice (Fig. 2B,
216 D), indicating that the NEN-induced current is partially mediated by ANT proteins.

217 **Figure 2: NEN induces partially ANT-mediated H^+ current in mouse heart mitoplasts. A)**
218 Diagram of mouse heart mitoplast isolation and preparation for whole-organelle inner
219 membrane electrophysiology. **B)** Representative whole-organelle electrophysiological traces of
220 H^+ current density in response to voltage ramp protocols performed on mouse heart mitoplasts.
221 Left, Wildtype; Right, ANT1 knockout. **C)** Quantification of NEN-induced H^+ current across
222 mitochondrial inner membrane before and after application of 1 µM CATR, a known ANT
223 inhibitor. Significances calculated by Student's unpaired t-test. **D)** Quantification of H^+ current
224 density induced by 500 nM NEN in wildtype and ANT1-knockout mouse heart mitoplasts.

225 Given this possibility of ANT-mediated uncoupling occurring in sperm, and the presence
226 of a unique isoform (ANT4) in sperm cells, we investigated whether ANT4 is indeed expressed in
227 the sperm mitochondria. Other investigators have proposed that ANT4 is expressed throughout
228 the sperm flagellum, and hypothesized that it may function in collaboration with glycolytic
229 enzymes to traffic ATP throughout the sperm flagellum (28). However, all other ANT isoforms
230 are expressed exclusively on the inner mitochondrial membrane, so a flagellar localization would
231 be surprising. Using immunocytochemistry and confocal microscopy, we found that when
232 excess primary antibody is used, some ANT4 staining is indeed seen throughout the flagellum
233 (Fig. S3F), but when primary antibody concentration is titrated down to an optimal

234 concentration, that staining is restricted to the midpiece in a similar distribution to that of the
235 inner mitochondrial membrane protein Cytochrome c oxidase (COXIV) (Fig. 3A-C). This ANT4
236 staining is not seen in non-permeabilized sperm (Fig. S3D), suggesting an exclusively
237 mitochondrial localization consistent with other ANT isoforms. To confirm this finding, we
238 conducted stochastic optical reconstruction microscopy (STORM) on human sperm cells similarly
239 costained for COXIV and ANT4 (Fig. 3D-F, top) and found that upon virtual cross-sectioning of
240 the midpiece, their distributions formed rings of similar diameter and thickness (Fig. 3D-F,
241 bottom), consistent with mitochondrial localization.

242 **Figure 3: ANT4 is localized to the human sperm mitochondria. A-C)** Confocal microscopy of
243 human sperm immunocytochemistry showing the localization of COXIV (magenta), ANT4
244 (green), and DAPI (blue) **D-F)** Stochastic optical reconstruction microscopy (STORM) of human
245 sperm cells showing the localization of COXIV (magenta) and ANT4 (green). Top panels:
246 overhead view (XY plane) of sperm cells. Bottom panels: virtual cross section (XZ plane) of
247 midpiece area indicated in top panels by white dotted box.

248 **Small molecule uncouplers do not reduce human sperm ATP content, and NEN induces**
249 **significant proton current across the sperm plasma membrane.**

250 To investigate the mechanism of action of NEN and BAM15's effect on sperm basal
251 motility (Fig. 1E, F) we assessed their effects on sperm ATP levels and found that neither
252 compound had any effect on ATP concentrations in noncapacitated (Fig. 4A) or capacitated (Fig.
253 4B) spermatozoa. Consistent with this finding, we observed that NEN and BAM15 had no effect
254 on other ATP-dependent human sperm physiological processes, including the acrosome
255 reaction, a necessary pre-fertilization exocytotic event (29,30) that exposes key fertilization

256 receptors (31,32) (Fig. S4A – C), and human sperm hyperactivated motility (33) (Fig. S4D, E).
257 NEN also did not impair *in vitro* fertilization between mouse sperm and eggs (Fig. S4F, G).

258 **Figure 4: Effects of small molecule uncouplers on human sperm ATP production and sperm**
259 **membrane proton current. A)** Left, quantification of ATP content of non-capacitated human
260 sperm treated with NEN, BAM15, and DMSO vehicle. Right, area under the curve analysis of the
261 plot to the left. **B)** Left, quantification of ATP content of human sperm capacitated in the
262 presence of NEN, BAM15, and DMSO vehicle. In both A and B, nonlinear regressions not shown,
263 because all adjusted R^2 values were <.1. Outliers in both A and B tested using a ROUT coefficient
264 of 1%, with no outliers detected. Error bars in all plots represent SEM. Statistical significance in
265 AUC analysis calculated using Dunnett's multiple comparisons test. **C)** Left, Representative
266 electrophysiological traces showing the effect of vehicles and uncouplers on human sperm
267 membrane H^+ current density. Right, diagram of sperm electrophysiology setup. Cytoplasmic
268 droplet is magnified for visibility. **D)** Quantification of maximal current densities in the presence
269 of 10µM NEN (left) and FCCP (right), at a voltage of -80mV. Error bars represent SEM, and
270 significance calculated using Tukey's Multiple Comparisons Test.

271

272 Since the uncouplers' negative effects on sperm basal motility were not mediated by a
273 reduced amount of cellular ATP, to further investigate their mechanism of action we assessed
274 the effects of each compound on sperm plasma membrane H^+-ion current using whole-cell
275 patch clamp electrophysiology. In this assay, 10 µM NEN and 10 µM FCCP induced a significant
276 inward transmembrane H^+-ion current at negative voltages (Fig. 4C, D), while 10 µM BAM15,
277 100 µM DNP, and the Ethanol and DMSO vehicles induced no discernable H^+ current (Fig. 4C,
278 S5A). The maximum current density of 10 µM FCCP (Fig. 4D) and 100 µM DNP (Fig. S5A) was

279 consistent with recently reported values in the plasma membrane of HEK293 cells (22).
280 Additionally, the current density induced by 10 µM NEN across the sperm plasma membrane
281 (Fig. 4D) was only roughly 1.5 times greater than the current density caused by a 20x lower
282 concentration of NEN in the inner mitochondrial membrane (IMM) (Fig. 2D). This buttresses the
283 idea that part of NEN's current is mediated by ANT proteins located exclusively in the IMM,
284 which increase the IMM's permeability to NEN-induced current. Although NEN took
285 significantly longer than FCCP to reach its maximal transmembrane current, their maximal rates
286 of change of current density were not significantly different, indicating that their mechanisms of
287 action may be similar (Fig. S5B, C).

288 **Discussion**

289

290 This study sheds light on several key aspects of sperm energetics and physiology.
291 There has been an ongoing debate in the field about whether oxidative phosphorylation or
292 glycolysis is the primary source of ATP for human spermatozoa (34–36), with increasing
293 evidence supporting the idea that glycolysis is sufficient to support many human sperm
294 functions (6). Our data support this conclusion, with both NEN and BAM15 failing to reduce
295 human sperm's ATP content or ability to undergo the acrosome reaction or hyperactivated
296 motility. Nonetheless, both uncouplers had an inhibitory effect on sperm basal motility, which
297 in the case of NEN is likely to be related to its induction of current across the sperm plasma
298 membrane (Fig. 4C, D), which would in turn affect many ion channels and intracellular signaling
299 pathways that rely on a carefully moderated membrane potential for proper function. Since
300 BAM15 is known as a more mitochondria-specific uncoupler (22,37–39) and did not induce
301 plasma membrane current in our sperm electrophysiology assays (Fig. 4C, S5A) the mechanism
302 of action of its more modest inhibition of basal progressive motility remains to be clarified. The

303 fact that DNP, a known mitochondrial uncoupler (22), failed to reduce mitochondrial membrane
304 potential may be related to DNP's low pK_a (23,40) limiting its permeability into living sperm cells
305 and/or the amount of current produced at pH 7.4, or due to the different complement of ANT
306 isoforms present in sperm mitochondria versus skeletal muscle mitochondria (16,17,41,42),
307 which may bind DNP with different affinites.

308 Although our study found that ANT4 was indeed mitochondrially localized and that the
309 ANT family of proteins can mediate NEN-induced uncoupling, our data suggest that
310 contraceptives that solely interfere with mature sperm oxidative phosphorylation will be
311 unlikely to successfully inhibit key sperm functions. However, pairing an oxidative
312 phosphorylation inhibitor with an inhibitor of a sperm-specific glycolytic enzyme, like lactate
313 dehydrogenase C (43), might produce an effective contraceptive product. Additionally, since
314 niclosamide has been FDA approved for use in humans with a favorable safety profile (24), and
315 possesses low bioavailability (44), a pK_a close to 6 (45) (close to the vaginal pH), and significant
316 deleterious effects on sperm motility, it could be an useful ingredient in on-demand vaginal
317 contraceptive products as an alternative to traditional nonoxynol 9-based spermicides.

318

319 **Materials and Methods**

320

321 All experiments were performed in accordance with NIH guidelines for animal research and
322 approved by UC Berkeley Animal Care and Use Committee (AUP 2015-07-7742), with every
323 effort made to minimize animal suffering. All described methods are consistent with the
324 recommendations of the Panel on Euthanasia of the American Veterinary Medical Association
325 and IACUC committee. All experimental procedures utilizing human derived samples were

326 approved by the Committee on Human Research at the University of California, Berkeley, IRB
327 protocol number 2013-06-5395.

328 **Reagents**

329 - Niclosamide Ethanolamine was purchased from AdipoGen Life Sciences,
330 #AG-CR1-3644
331 - BAM15 was purchased from Sigma, product number SML1760-5MG
332 - 2,4, dinitrophenol was purchased from TCI, product D0109-25G
333 - FCCP was purchased from abcam, product code ab120081.
334 - Mitotracker Red CMXRos was purchased from ThermoFisher, #M7512
335 - Polyclonal Antibody to human ANT4 – Novus Biologicals NBP1-89074
336 raised in Rabbits against human ANT4 peptide
337 - Mouse Monoclonal Antibody against human COX4I1 – Proteintech
338 #66110-1-Ig
339 - Polyvinyl Alcohol was purchased from Fluka, #81366-100G
340 - A23187 was purchased from MilliporeSigma, #C7522-5MG.
341 - 10% Goat Serum from Invitrogen, #50-062Z
342 - Bovine Serum Albumin from Sigma, #A3059-500G
343

344 **Sperm Preparation**

345 Human sperm cells were collected by masturbation from healthy donors and visually inspected
346 for normal morphology and motility before use. Spermatozoa were isolated by the swim-up

347 procedure in HTF or HS solution as previously described (46) and then concentrated by 5 minute
348 centrifugation at ≤500g and supernatant removal.

349 **Flow Cytometric Assessment of MMP**

350 Human sperm cells were incubated with small molecule uncouplers or vehicles in HS solution for
351 30 minutes at 37°C , then treated with 50nM MitoTracker Red in the presence of either
352 uncouplers or vehicles for an additional 30 minutes. Subsequently, cells were washed by
353 centrifugation for 5 minutes at 500 g, supernatant was removed, and cells were resuspended in
354 HS solution. Fluorescence was measured by flow cytometry on a BD LSR Fortessa Celeste or BD
355 LSR Fortessa X20, using gates for size and density to exclude debris and aggregates, and a PE-
356 Texas Red Filter set (561nm laser excitation, 610/20 nm emission filter) to record fluorescence
357 (Fig. 1, S1). Fluorescence midpiece location was confirmed by microphotography on an Olympus
358 IX71 inverted microscope using a Hamamatsu Orca-ER digital camera, and a 60x Olympus
359 UPlanSApo objective (Fig. 1). Fluorescence statistics were analyzed using Microsoft Excel
360 version 16 and GraphPad Prism version 9. The subpopulation of cells with the highest gaussian
361 distribution of fluorescence were manually gated and the mean fluorescence of this population
362 was normalized to the average of the means of the same population in the relevant vehicle
363 control samples of each run. Each data point represents the mean fluorescence of the highest
364 normally peak in an individual flow cytometry run of 10,000 cells. Nonlinear least squares
365 regression performed using an unweighted [inhibitor] vs. response three parameter model (Hill
366 Slope = -1.0), identifying “unstable” fits. Outliers tested using a ROUT coefficient of 1%, with no
367 outliers detected. Residuals were checked for normality using the D’Agostino-Pearson omnibus
368 normality test, checked for clustering using the Replicates test, and checked for appropriate

369 weighting using the homoscedasticity test, and passed all tests, except for FCCP which failed the
370 test for homoscedasticity.

371 **Area Under the Curve Analysis**

372 **F**or all dose-response plots, Area Under the Curve (AUC) analysis was performed using the
373 trapezoid method ($\Delta X*(Y_1+Y_2)/2$) on the arithmetic means of the measured parameter at each
374 compound concentration. Each data point represents the area under the curve of all
375 concentrations tested in one biological replicate. Effects of each compound were then
376 compared using Dunnett's Multiple Comparison's Test.

377 **Sperm Motility Assessment**

378 Isolated human sperm were incubated with small molecule uncouplers and vehicles at 37°C for
379 30 minutes, after which they were mixed with 1% Polyvinyl Alcohol to prevent adherence to
380 glass and loaded into a Leja Standard Count 2-chamber sperm analysis slide (depth 20 micron).
381 Sperm motility was analyzed on a Hamilton-Thorne IVOS I computer-aided sperm analyzer, at
382 37°C. Motility was measured for least 500 cells in each condition. Progressive motility was
383 defined using Hamilton-Thorne's proprietary software module. Nonlinear least squares
384 regression performed by GraphPad Prism version 9 using an unweighted [inhibitor] vs. response
385 three parameter model (Hill Slope = -1.0), identifying "unstable" fits. Outliers were tested using
386 a ROUT coefficient of 1% and none were identified. Residuals were checked for normality using
387 the D'Agostino-Pearson omnibus normality test, checked for clustering using the Replicates test,
388 and checked for appropriate weighting using the homoscedasticity test. Residuals for NEN and
389 BAM15 passed all tests, except that BAM15 failed the test for homoscedasticity with a p-value
390 of 0.0207.

391 Human sperm hyperactivated motility was measured on a Hamilton-Thorne IVOS II computer-
392 aided sperm analyzer, as above, with the definition for hyperactivated motility set as VCL
393 >150 µm/s AND LIN <50% AND ALH >7.0 µm (33).

394 **Flow Cytometric Assessment of Acrosome Status**

395 Human sperm cells were incubated for 3.5 hours in capacitation media (20% Fetal Bovine Serum
396 and 25mM Sodium Bicarbonate in HS solution) at 37°C and 5% CO_2. In the final hour of
397 incubation, custom monoclonal antibodies raised in mouse hybridoma cells against the
398 ectodomain of human Izumo1 were added, at a concentration of 10µg/mL. Subsequently 50µM
399 A23187 was added, and cells were incubated at 37°C and 5% CO_2 for an additional 30 minutes,
400 after which cells were washed by centrifugation 3x (500 g, 5 min) in HS solution, incubated 30
401 minutes at room temperature with a goat anti-mouse 647 secondary antibody (Invitrogen
402 A32728, final concentration 4µg/mL) in 10% goat serum. After an additional 3 washes by
403 centrifugation, propidium iodide (PI) was added to a final concentration of 1µg/mL, and cells
404 were analyzed by flow cytometry using the same instrumentation as above, except that Izumo-
405 647 was visualized using an APC filter set (bandpass 670/30 or 670/14nm) and Propidium Iodide
406 was visualized using a PE-Texas Red filter set (bandpass 610/20nm). Izumo-647 positive cells
407 were scored as acrosome reacted, and PI negative cells were scored as living.

408 **Generation of IZUMO1 monoclonal antibody using mouse hybridoma**

409 The IZUMO1 monoclonal antibodies were generated from mouse hybridoma and characterized
410 as previously described (47). Briefly, IZUMO1 antibodies 4E04 and 6F02 belong to the murine
411 IgG1 isotype with kappa light chain. For antibody production, hIZUMO1-positive hybridomas
412 were cultured in medium containing 10% FBS and subsequently adapted to an FBS-free medium.

413 The condition media were harvested, and the IgG antibody were purified by protein G affinity
414 chromatography and by Superdex-200 gel filtration chromatography in a buffer of 150 mM NaCl,
415 20 mM HEPES pH 7.4. Purified IgG antibodies were concentrated to 1 mg/mL with the addition
416 of 10% (v/v) glycerol for use.

417 **ATP Assessment**

418 Human Sperm cells were incubated with uncoupler compounds or vehicle for 1 hour at 37°C in
419 white 96-well Costar polystyrene assay plates, under sterile conditions. ATP content was
420 assessed using a PerkinElmer ATPlite Luminescence Assay System Kit, according to manufacturer
421 instructions, and luminescence was imaged on a Biotek Synergy H4 Hybrid plate reader, set to
422 endpoint/kinetic setting (one measurement point per well), with 1 second of integration time
423 and a manual gain setting of 135. ATP content was quantified by interpolating against a
424 standard curve of ATP solutions, per manufacturer instructions. Nonlinear least squares
425 regression performed by GraphPad Prism version 9 using an [inhibitor] vs. response three
426 parameter model (Hill Slope = -1.0), weighted by $1/Y^2$, identifying "ambiguous" fits. Outliers
427 tested using a ROUT coefficient of 1%, with no outliers detected. Residuals were checked for
428 normality using the D'Agostino-Pearson omnibus normality test, checked for clustering using the
429 Replicates test, and checked for appropriate weighting using the homoscedasticity test, and
430 passed all tests.

431 **Mouse In Vitro Fertilization**

432 All mice were kept in the Animal Facility of the University of California, Berkeley, fed standard
433 chow diet (PicoLab Rodent diet 20, #5053, LabDiet), and hyper-chlorinated water *ad libitum* in a
434 room with controlled light (14 hours light, 10 hours darkness) and temperature (23±0.5°C).

435 Animals were humanely killed by CO_2 asphyxiation and cervical dislocation according to ACUC
436 guidelines with every effort made to minimize suffering.

437 C57Bl/6N (Charles River) female mice between 4 and 16 weeks old were superovulated by
438 intraperitoneal injection of 5 IU pregnant mare serum gonadotropin (PMSG, Sigma, G4877) and
439 48 hours later, 5 IU human chorionic gonadotropin (hCG, Millipore, 230734). 13 hours after hCG
440 injection the females were euthanized and cumulus-oocyte complexes were collected from the
441 oviduct ampulla in HTF medium (Embryomax, Specialty Media, Millipore) and incubated for 30
442 minutes at 37°C and 5% CO_2 prior to insemination. Simultaneously, mouse sperm were isolated
443 from the cauda epididymis as previously described[36] and allowed to capacitate at 37°C and 5%
444 CO_2 for 60-90 minutes in the presence of uncoupler compounds or control vehicle. Sperm and
445 eggs were then mixed to a final concentration of 210,000 sperm/mL in 600µL of HTF medium
446 and incubated at 37°C and 5% CO_2 for 4 hours. Afterwards, the eggs were washed by mouth
447 pipetting in HTF media to remove excess sperm. A final wash in KSOM media (Zenith Biotech)
448 supplemented with 1mg/mL BSA was then done before dividing the eggs into 10 µl drops of
449 KSOM/BSA media overlaid with embryo-tested light mineral oil (Millipore) for culture at 37°C,
450 5% CO_2. Best efforts were made to divide equal numbers of eggs from each mouse into control
451 and uncoupler-treated conditions. 3.5 days following IVF, the number of fertilized eggs was
452 determined visually by assessing the percentage of embryos that reached morula or blastula
453 stage.

454 **Sperm Whole-Cell Electrophysiology**

455 Whole-cell electrophysiology was performed on isolated human sperm cells as described
456 previously (48,49). Once sperm cell "break in" was achieved in HS solution, cells were subjected
457 to a voltage ramp protocol in the presence of bath and pipette solutions designed to ensure that

458 only H^+ current across the membrane was measured. Intracellular (pipette) solution contained:
459 150mM NMDG, 5mM BAPTA, 100mM HEPES, 1mM Tris Chloride, pH 7.5 with $MeSO_3$.
460 Extracellular (bath) solution contained: 157mM NMDG, 20mM MES, 1mM $MgCl_2$, 100µM $ZnCl_2$,
461 pH 6 with $MeSO_3$. Compounds and vehicles were applied by perfusion, and currents were
462 recorded until they showed a minimal change between subsequent voltage ramps. Then,
463 compounds were washed out, and subsequent compounds added once currents had returned to
464 baseline values. Representative traces and time courses created in Origin Pro version 9.0.0 and
465 statistical analysis performed in GraphPad Prism 9.

466 **Mitochondrial Patch-Clamp Electrophysiology**

467 Mouse heart mitochondria were isolated from wildtype and $ANT1^{-/-}$ C57BL/6J2z mice and
468 mitoplasts prepared and patch-clamped as described previously (21). Both the bath and pipette
469 solutions were formulated to record H^+ currents and contained only salts that dissociate into
470 large anions and cations that are normally impermeant through ion channels or transporters.
471 Pipettes were filled with 130 mM tetramethylammonium hydroxide (TMA), 1.5 mM EGTA, 2 mM
472 Tris chloride, and 100 mM HEPES (or MES). pH was adjusted to 7.5 with d-gluconic acid, and
473 tonicity was adjusted to ∼360 mmol/kg with sucrose. Bath solution contained 100 mM HEPES
474 (or MES) and 1 mM EGTA (pH adjusted to 7.0 with Trizma base, and tonicity adjusted to ∼300
475 mmol/kg with sucrose).

476 **Immunocytochemistry**

477 Briefly, sperm were adhered onto poly-D-Lysine coated coverslips, and, in some experiments,
478 incubated 15 minutes at 37°C with 50 nM MitoTracker Red CMXRos, then washed and fixed in
479 4% PFA for 10 minutes, and washed and additionally fixed in ice-cold methanol for 1 minute.

480 Cells were permeabilized and blocked in 5% BSA and 0.1% Triton X-100 in PBS for 45 minutes,
481 then incubated overnight at 4°C with rabbit polyclonal antibody against Human ANT4 (Novus
482 #NBP1-89074, used at .08 µg/mL) and, in some experiments, a mouse monoclonal antibody
483 against COXIV (COX4l1) (Proteintech #66110-1-Ig, used at 6.8µg/mL). After washing, samples
484 were incubated with secondary antibodies (Jackson Alexa Fluor 647 AffiniPure Donkey Anti-
485 Rabbit IgG (H+L) (code 711-605-152) at a dilution of 1:1000, and Jackson ImmuoResearch anti-
486 mouse Cy3 or Molecular Probes A10521 goat anti-mouse Cy3 at a dilution of 1:1000) for 45
487 minutes, then washed and mounted using ProLong Gold Antifade mountant with DAPI.

488 Cells were imaged on an Olympus FV3000 inverted laser scanning confocal microscope, using a
489 Olympus UPLSAPO Super Apochromat 60x oil immersion objective (NA 1.35) and Olympus Z-
490 81226 immersion oil. Laser Scanning was performed by galvanometer, unidirectionally at a rate
491 of 2µs/pixel with no averaging, with pixel sizes of .207 µm/pixel in the x and y direction.
492 Multiple colors were imaged in line-by-line sequential scanning mode, and multiple z-planes
493 were acquired with a thickness of .47 µm, on a linear-encoded stage. Images displayed are
494 maximum intensity z-stacks of all relevant z-planes. All colors were imaged with a pinhole
495 diameter of 233 µM, and laser illumination was passed through a 10% neutral density filter.
496 DAPI was illuminated by a 405 nm laser set to 3% power, and emitted light was passed through
497 a 430-470 nm emission filter and detected with a photomultiplier tube (PMT) set to 500V. Cy3
498 was illuminated by a 561 nm laser set to 4% power, with a 570-620 nm emission filter and a PMT
499 set to 500V. Alexa 674 was illuminated by a 642 nm laser set to 4% power, with a 650-750 nm
500 emission filter and a PMT set to 550V.

501 **Super-resolution Microscopy**

502 ICC slides made as described above were imaged using three-dimensional stochastic optical
503 reconstruction microscopy (3D-STORM) (50,51) performed on a home-built set-up using a Nikon
504 CFI Plan Apo λ 100× oil immersion objective (NA 1.45), as described previously (52). In brief, the
505 sample was mounted with an imaging buffer consisting of 5% (w/v) glucose, 100 mM
506 cysteamine, 0.8 mg ml^{-1} glucose oxidase and 40 µg ml^{-1} catalase in a Tris HCl buffer (pH 7.5). For
507 two-color imaging of COXIV and ANT4, the two targets were labeled by Alexa Fluor 647 and
508 CF568, respectively, and were imaged sequentially using 647- and 560-nm excitation lasers.
509 These lasers were passed through an acousto-optic tunable filter and illuminated a few
510 micrometers into the sample at around 2 kW cm^{-2}, thus photoswitching most of the labeled dye
511 molecules in the sample into the dark state while allowing a small, random fraction of molecules
512 to emit across the wide-field over different camera frames. Single-molecule emission was
513 passed through a cylindrical lens of focal length 1 m to introduce astigmatism (51), and recorded
514 with an Andor iXon Ultra 897 EM-CCD camera at a frame rate of 110 Hz, for a total of around
515 50,000 frames per image. Data acquisition used publicly available software
516 (https://github.com/ZhuangLab/storm-control). The raw STORM data were analyzed using
517 Insight3 software (51) according to previously described methods (50,51). Secondary antibodies
518 used: Alexa Fluor 647-labelled goat anti-mouse (Invitrogen, A21236, 1:400) and donkey anti-
519 rabbit (Jackson ImmunoResearch, 711-005-152, 1:70) conjugated with CF568 succinimidyl ester
520 (Biotium, 92131).

521 **Western Blotting**

522 Human Sperm or HEK293 cells were lysed by addition of $RIPA^{++}$ Buffer (composition: 50mM Tris
523 HCl, pH 7.4; 150mM NaCl; 1% Triton X-100; 0.5% Sodium Deoxylcholate; 0.1% Sodium Dodecyl
524 Sulfate; 1 mM EDTA; 10% glycerol; with Pierce Protease inhibitor tablet or solution added to

525 manufacturer's instructions), then homogenized by 25 passes through a 21-gauge or smaller
526 syringe, then shook on ice for 30 minutes, and centrifuged at 12000 rpm at 4°C for 20 minutes,
527 after which the supernatant was collected and frozen at -80°C. After thawing, protein
528 concentration was assessed using a Pierce Rapid Gold BCA Protein Assay Kit, per manufacturer
529 instructions, and measured on a Biotek Synergy H4 Hybrid plate reader. A target of 30µg of
530 protein was mixed with 4x Laemmli Buffer and Beta-Mercaptoethanol, heated for 10 minutes at
531 99°C, then loaded to each well of a precast 4-20% mini-Protean TGX gel (Bio-Rad), and run in an
532 electrophoresis chamber until ladder bands were well-resolved. Transfer onto a PVDF
533 membrane was accomplished with an Invitrogen iBlot Dry Blotting System, following
534 manufacturer instructions, at 20V for 7 minutes. After washing 3x with PBS with 0.1% Tween
535 (PBST), the membrane was blocked in 3% Bovine Serum Albumin for 15-30 minutes, then
536 incubated rocking with primary antibody overnight at 4°C. The following day, the membrane
537 was washed 3x with PBST, and incubated with a 1:15000 dilution of HRP-conjugated Abcam
538 Ab6721 Goat pAb anti-Rabbit IgG secondary antibody for one hour at room temperature. After
539 3x PBST washes and 2x PBS washes, bands were visualized using a Prometheus ProSignal Pico
540 kit, per instructions, and imaged in a ProteinSimple FluorChem M. Afterwards, images were
541 inverted, rotated, and cropped in ImageJ 1.52a.

542 **Acknowledgments:**

543 This work was furthered by the support and guidance of Dr. Denise Schichnes, using the
544 equipment of the CNR Biological Imaging Facility at the University of California, Berkeley.
545 Research reported in this publication was supported in part by the National Institutes of Health
546 S10 program under award number 1S10OD018136-01. The content is solely the responsibility of
547 the authors and does not necessarily represent the official views of the National Institute of

548 Health. The authors also wish to thank Dr. Liliya Gabelev Khasin, Dr. Caroline Williams, and Dr.
549 Lisa Treidel, and Dr. Erwin Goldberg for their assistance with this project.

550 This work was supported by an NSF Graduate Research Fellowship and the Irving H.
551 Wiesenfeld Fellowship administered by the UC Berkeley Center for Emerging and Neglected
552 Diseases to W.M.S., a Male Contraceptive Initiative Graduate Fellowship to P.V.L. and Liliya
553 Gabelev Khasin, NIH NICHD grant K99HD104924 to S.T., NIGMS grant R35GM136415 to Y.K. ,
554 Pew Biomedical Scholars Award to P.V.L. and K.X. and Bakar Fellow Spark Award to P.V.L.

555 **References**

556 1. Suarez SS, Pacey AA. Sperm transport in the female reproductive tract. Hum Reprod Update.
557 2006 Jan 1;12(1):23–37.

558 2. Suarez SS. Mammalian Sperm Interactions with the Female Reproductive Tract. Cell Tissue
559 Res. 2016 Jan;363(1):185–94.

560 3. Turner RM. Moving to the beat: a review of mammalian sperm motility regulation. Reprod
561 Fertil Dev. 2006;18(2):25.

562 4. Suarez SS. Control of hyperactivation in sperm. Hum Reprod Update. 2008 Nov 1;14(6):647–
563 57.

564 5. Mundy AJ, Ryder TA, Edmonds DK. Asthenozoospermia and the human sperm mid-piece.
565 Hum Reprod. 1995 Jan 1;10(1):116–9.

566 6. Hereng TH, Elgstøen KBP, Cederkvist FH, Eide L, Jahnsen T, Skålhegg BS, et al. Exogenous
567 pyruvate accelerates glycolysis and promotes capacitation in human spermatozoa. Hum
568 Reprod. 2011 Dec 1;26(12):3249–63.

569 7. Gallon F, Marchetti C, Jouy N, Marchetti P. The functionality of mitochondria differentiates
570 human spermatozoa with high and low fertilizing capability. Fertil Steril. 2006
571 Nov;86(5):1526–30.

572 8. Paoli D, Gallo M, Rizzo F, Baldi E, Francavilla S, Lenzi A, et al. Mitochondrial membrane
573 potential profile and its correlation with increasing sperm motility. Fertil Steril. 2011 Jun
574 1;95(7):2315–9.

575 9. Boguenet M, Bouet PE, Spiers A, Reynier P, May-Panloup P. Mitochondria: their role in
576 spermatozoa and in male infertility. Hum Reprod Update [Internet]. 2021 Feb 8 [cited 2021
577 Apr 26];(dmab001). Available from: https://doi.org/10.1093/humupd/dmab001

578 10. Zhang G, Wang Z, Ling X, Zou P, Yang H, Chen Q, et al. Mitochondrial Biomarkers Reflect
579 Semen Quality: Results from the MARCHS Study in Chongqing, China. PLOS ONE. 2016 Dec
580 22;11(12):e0168823.

581 11. Piomboni P, Focarelli R, Stendardi A, Ferramosca A, Zara V. The role of mitochondria in
582 energy production for human sperm motility: Mitochondria functionality in human
583 spermatozoa. Int J Androl. 2012 Apr;35(2):109–24.

584 12. Rodić N, Oka M, Hamazaki T, Murawski MR, Jorgensen M, Maatouk DM, et al. DNA
585 Methylation Is Required for Silencing of Ant4, an Adenine Nucleotide Translocase Selectively
586 Expressed in Mouse Embryonic Stem Cells and Germ Cells. STEM CELLS. 2005;23(9):1314–
587 23.

588 13. Zheng LP, Wang HF, Li BM, Zeng XH. Sperm-specific ion channels: targets holding the most
589 potential for male contraceptives in development. Contraception. 2013 Oct;88(4):485–91.

590 14. Noda T, Lu Y, Fujihara Y, Oura S, Koyano T, Kobayashi S, et al. Sperm proteins SOF1,
591 TMEM95, and SPACA6 are required for sperm−oocyte fusion in mice. Proc Natl Acad Sci.
592 2020 May 26;117(21):11493–502.

593 15. Leung MR, Chiozzi RZ, Roelofs MC, Hevler JF, Ravi RT, Maitan P, et al. In-cell structures of
594 conserved supramolecular protein arrays at the mitochondria–cytoskeleton interface in
595 mammalian sperm. Proc Natl Acad Sci [Internet]. 2021 Nov 9 [cited 2021 Nov 9];118(45).
596 Available from: https://www.pnas.org/content/118/45/e2110996118

597 16. Lim CH, Brower JV, Resnick JL, Oh SP, Terada N. Adenine Nucleotide Translocase 4 Is
598 Expressed Within Embryonic Ovaries and Dispensable During Oogenesis. Reprod Sci. 2015
599 Feb;22(2):250–7.

600 17. Brower JV, Rodic N, Seki T, Jorgensen M, Fliess N, Yachnis AT, et al. Evolutionarily Conserved
601 Mammalian Adenine Nucleotide Translocase 4 Is Essential for Spermatogenesis. J Biol
602 Chem. 2007 Oct 5;282(40):29658–66.

603 18. Hamazaki T, Leung WY, Cain BD, Ostrov DA, Thorsness PE, Terada N. Functional Expression
604 of Human Adenine Nucleotide Translocase 4 in Saccharomyces Cerevisiae. PLOS ONE. 2011
605 Apr 21;6(4):e19250.

606 19. Leung WY, Hamazaki T, Ostrov DA, Terada N. Identification of adenine nucleotide
607 translocase 4 inhibitors by molecular docking. J Mol Graph Model [Internet]. 2013 Sep [cited
608 2018 Jun 12];45. Available from: https://www.ncbi.nlm.nih.gov/pmc/articles/PMC3821932/

609 20. Zhang Y, Tian D, Matsuyama H, Hamazaki T, Shiratsuchi T, Terada N, et al. Human Adenine
610 Nucleotide Translocase (ANT) Modulators Identified by High-Throughput Screening of
611 Transgenic Yeast. J Biomol Screen. 2016 Apr;21(4):381–90.

612 21. Bertholet AM, Chouchani ET, Kazak L, Angelin A, Fedorenko A, Long JZ, et al. H + transport is
613 an integral function of the mitochondrial ADP/ATP carrier. Nature. 2019 Jul;571(7766):515.

614 22. Bertholet AM, Natale AM, Bisignano P, Suzuki J, Fedorenko A, Hamilton J, et al.
615 Mitochondrial uncouplers induce proton leak by activating AAC and UCP1. Nature. 2022
616 Jun;606(7912):180–7.

617 23. Childress ES, Alexopoulos SJ, Hoehn KL, Santos WL. Small Molecule Mitochondrial
618 Uncouplers and Their Therapeutic Potential: Miniperspective. J Med Chem. 2018 Jun
619 14;61(11):4641–55.

620 24. Kadri H, Lambourne OA, Mehellou Y. Niclosamide, a Drug with Many (Re)purposes.
621 ChemMedChem. 2018;13(11):1088–91.

622 25. World Health Organization. WHO laboratory manual for the examination and processing of
623 human semen [Internet]. 6th ed. Geneva: World Health Organization; 2021 [cited 2021 Nov
624 11]. Available from: https://apps.who.int/iris/handle/10665/343208

625 26. Dolce V, Scarcia P, Iacopetta D, Palmieri F. A fourth ADP/ATP carrier isoform in man:
626 identification, bacterial expression, functional characterization and tissue distribution. FEBS
627 Lett. 2005 Jan 31;579(3):633–7.

628 27. Levy SE, Chen YS, Graham BH, Wallace DC. Expression and sequence analysis of the mouse
629 adenine nucleotide translocase 1 and 2 genes. Gene. 2000 Aug;254(1–2):57–66.

630 28. Kim YH, Haidl G, Schaefer M, Egner U, Mandal A, Herr JC. Compartmentalization of a unique
631 ADP/ATP carrier protein SFEC (Sperm Flagellar Energy Carrier, AAC4) with glycolytic
632 enzymes in the fibrous sheath of the human sperm flagellar principal piece. Dev Biol. 2007
633 Feb;302(2):463–76.

634 29. Brucker C, Lipford GB. The human sperm acrosome reaction: physiology and regulatory
635 mechanisms. An update. Hum Reprod Update. 1995 Jan;1(1):51–62.

636 30. Hirohashi N, Yanagimachi R. Sperm acrosome reaction: its site and role in fertilization†. Biol
637 Reprod. 2018 Feb;99(1):127–33.

638 31. Satouh Y, Inoue N, Ikawa M, Okabe M. Visualization of the moment of mouse sperm–egg
639 fusion and dynamic localization of IZUMO1. J Cell Sci. 2012 Nov 1;125(21):4985–90.

640 32. Balestrini PA, Jabloñski M, Schiavi-Ehrenhaus LJ, Marín-Briggiler CI, Sánchez-Cárdenas C,
641 Darszon A, et al. Seeing is believing: Current methods to observe sperm acrosomal
642 exocytosis in real time. Mol Reprod Dev. 2020;87(12):1188–98.

643 33. Mortimer ST, van der Horst G, Mortimer D. The future of computer-aided sperm analysis.
644 Asian J Androl. 2015;17(4):545–53.

645 34. du Plessis SS, Agarwal A, Mohanty G, van der Linde M. Oxidative phosphorylation versus
646 glycolysis: what fuel do spermatozoa use? Asian J Androl. 2015;17(2):230–5.

647 35. Ford WCL. Glycolysis and sperm motility: does a spoonful of sugar help the flagellum go
648 round? Hum Reprod Update. 2006 Jun 1;12(3):269–74.

649 36. Storey BT. Mammalian sperm metabolism: oxygen and sugar, friend and foe. Int J Dev Biol.
650 2008;52(5–6):427–37.

651 37. Kenwood BM, Weaver JL, Bajwa A, Poon IK, Byrne FL, Murrow BA, et al. Identification of a
652 novel mitochondrial uncoupler that does not depolarize the plasma membrane. Mol Metab.
653 2014 Apr 1;3(2):114–23.

654 38. Kenwood BM, Calderone JA, Taddeo EP, Hoehn KL, Santos WL. Structure–activity
655 relationships of furazano[3,4-b]pyrazines as mitochondrial uncouplers. Bioorg Med Chem
656 Lett. 2015 Nov 1;25(21):4858–61.

657 39. Firsov AM, Popova LB, Khailova LS, Nazarov PA, Kotova EA, Antonenko YN. Protonophoric
658 action of BAM15 on planar bilayers, liposomes, mitochondria, bacteria and neurons.
659 Bioelectrochemistry. 2021 Feb 1;137:107673.

660 40. Hopfer U, Lehninger AL, Thompson TE. Protonic conductance across phospholipid bilayer
661 membranes induced by uncoupling agents for oxidative phosphorylation. Proc Natl Acad Sci.
662 1968 Feb 1;59(2):484–90.

663 41. Stepien G, Torroni A, Chung AB, Hodge JA, Wallace DC. Differential expression of adenine
664 nucleotide translocator isoforms in mammalian tissues and during muscle cell
665 differentiation. J Biol Chem. 1992 Jul 25;267(21):14592–7.

666 42. Doerner A, Pauschinger M, Badorff A, Noutsias M, Giessen S, Schulze K, et al. Tissue-specific
667 transcription pattern of the adenine nucleotide translocase isoforms in humans. FEBS Lett.
668 1997 Sep 8;414(2):258–62.

669 43. Goldberg E. The Sperm Specific Form of Lactate Dehydrogenase (LDHC4) is Required for
670 Fertility and is an Attractive Target for Male Contraception (A Review). Biol Reprod
671 [Internet]. 2020 [cited 2020 Dec 2]; Available from:
672 https://academic.oup.com/biolreprod/advance-
673 article/doi/10.1093/biolre/ioaa217/6008540

674 44. Zhang X, Zhang Y, Zhang T, Zhang J, Wu B. Significantly enhanced bioavailability of
675 niclosamide through submicron lipid emulsions with or without PEG-lipid: a comparative
676 study. J Microencapsul. 2015 Jul 4;32(5):496–502.

677 45. Jurgeit A, McDowell R, Moese S, Meldrum E, Schwendener R, Greber UF. Niclosamide Is a
678 Proton Carrier and Targets Acidic Endosomes with Broad Antiviral Effects. PLoS Pathog
679 [Internet]. 2012 Oct 25 [cited 2020 Aug 18];8(10). Available from:
680 https://www.ncbi.nlm.nih.gov/pmc/articles/PMC3486884/

681 46. Skinner WM, Mannowetz N, Lishko PV, Roan NR. Single-cell Motility Analysis of Tethered
682 Human Spermatozoa. Bio-Protoc [Internet]. 2019 Mar 5 [cited 2019 May 7];9(5). Available
683 from: https://www.ncbi.nlm.nih.gov/pmc/articles/PMC6482966/

684 47. Tang S, Lu Y, Skinner WM, Sanyal M, Lishko PV, Ikawa M, et al. Human sperm TMEM95 binds
685 eggs and facilitates membrane fusion [Internet]. bioRxiv; 2022 [cited 2022 Jul 9]. p.

686 2022.06.10.495573. Available from:
687 https://www.biorxiv.org/content/10.1101/2022.06.10.495573v1

688 48. Liu B, Mundt N, Miller M, Clapham DE, Kirichok Y, Lishko PV. Recording Electrical Currents
689 across the Plasma Membrane of Mammalian Sperm Cells. JoVE J Vis Exp. 2021 Feb
690 14;(168):e62049.

691 49. Kirichok Y, Lishko PV. Rediscovering sperm ion channels with the patch-clamp technique.
692 MHR Basic Sci Reprod Med. 2011 Aug 1;17(8):478–99.

693 50. Rust MJ, Bates M, Zhuang X. Sub-diffraction-limit imaging by stochastic optical
694 reconstruction microscopy (STORM). Nat Methods. 2006 Oct;3(10):793–6.

695 51. Huang B, Wang W, Bates M, Zhuang X. Three-Dimensional Super-Resolution Imaging by
696 Stochastic Optical Reconstruction Microscopy. Science. 2008 Feb 8;319(5864):810–3.

697 52. Wojcik M, Hauser M, Li W, Moon S, Xu K. Graphene-enabled electron microscopy and
698 correlated super-resolution microscopy of wet cells. Nat Commun. 2015 Jun 11;6(1):7384.

Figures

Figure 1: Representative small-molecule uncouplers dose-dependently reduce sperm mitochondrial membrane potential and basal motility.

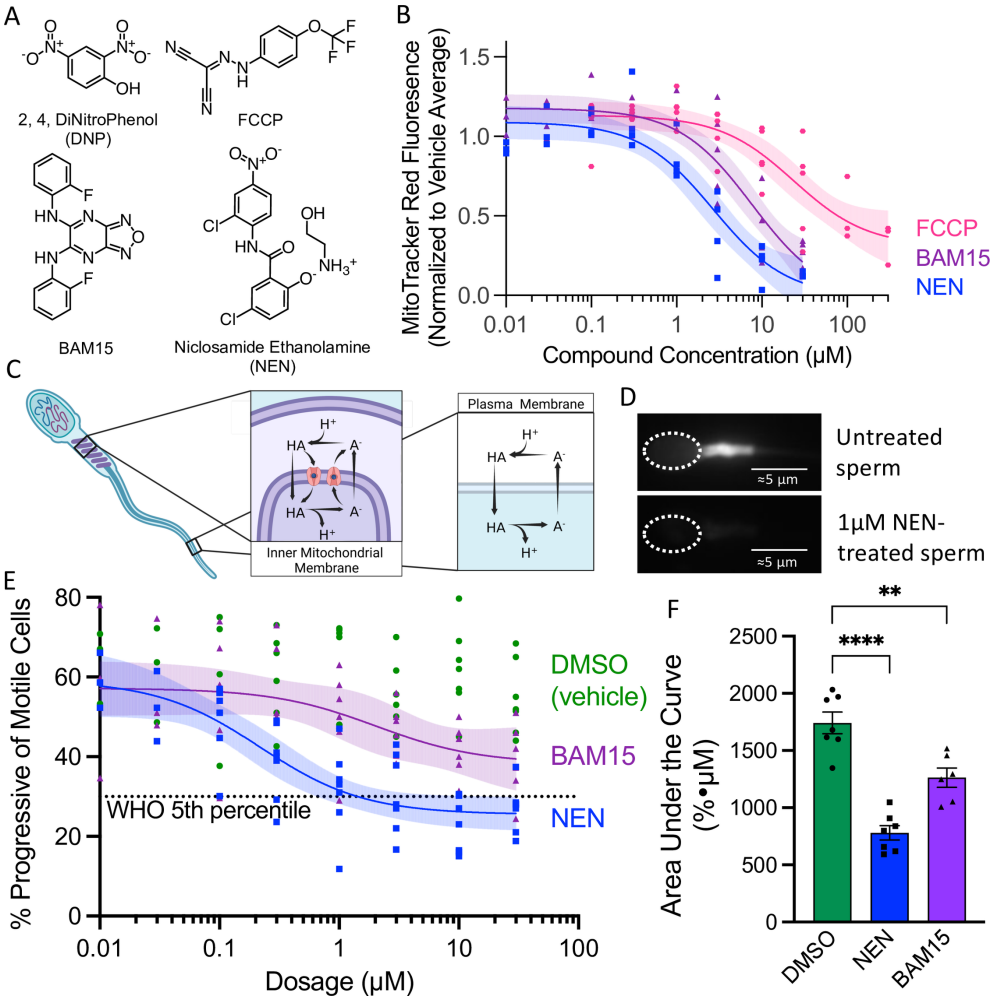

706 **Figure 2: NEN induces partially ANT-mediated H^+ current in mouse heart mitoplasts.**

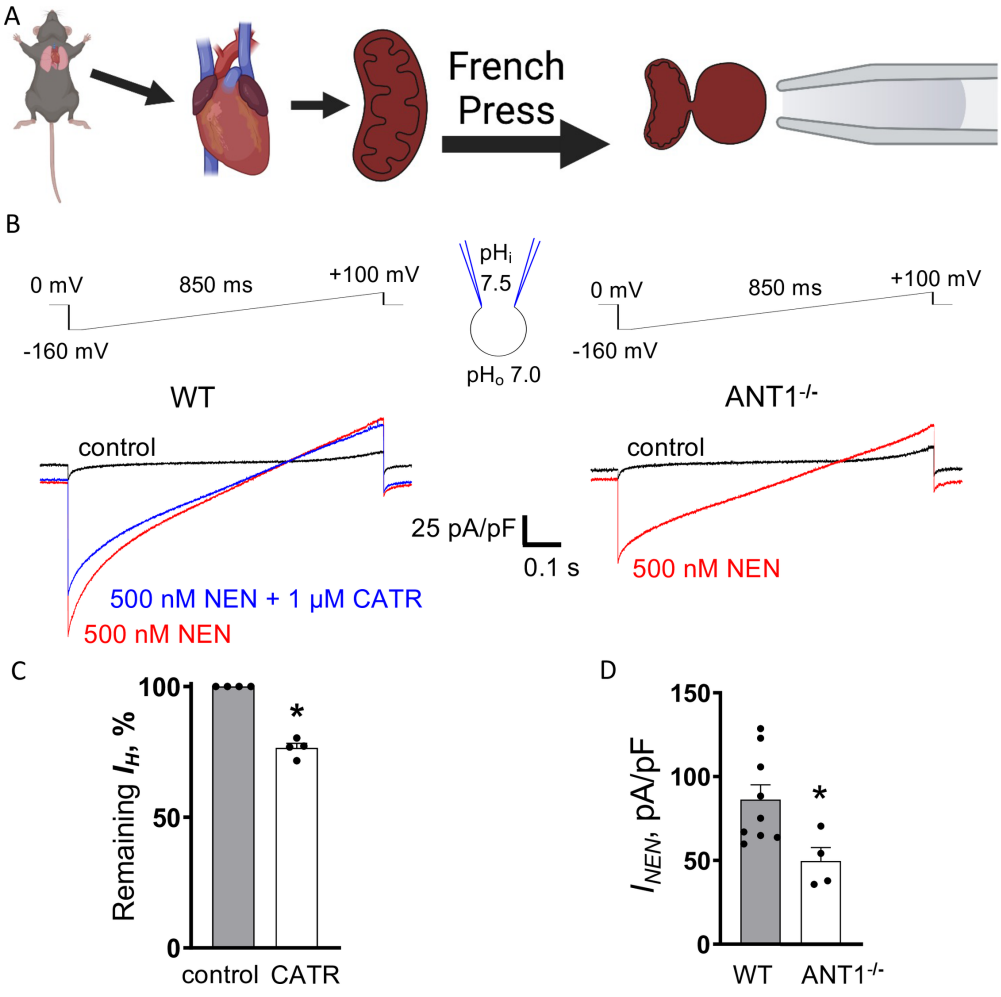

707

708 **Figure 3: ANT4 is localized to the human sperm mitochondria.**

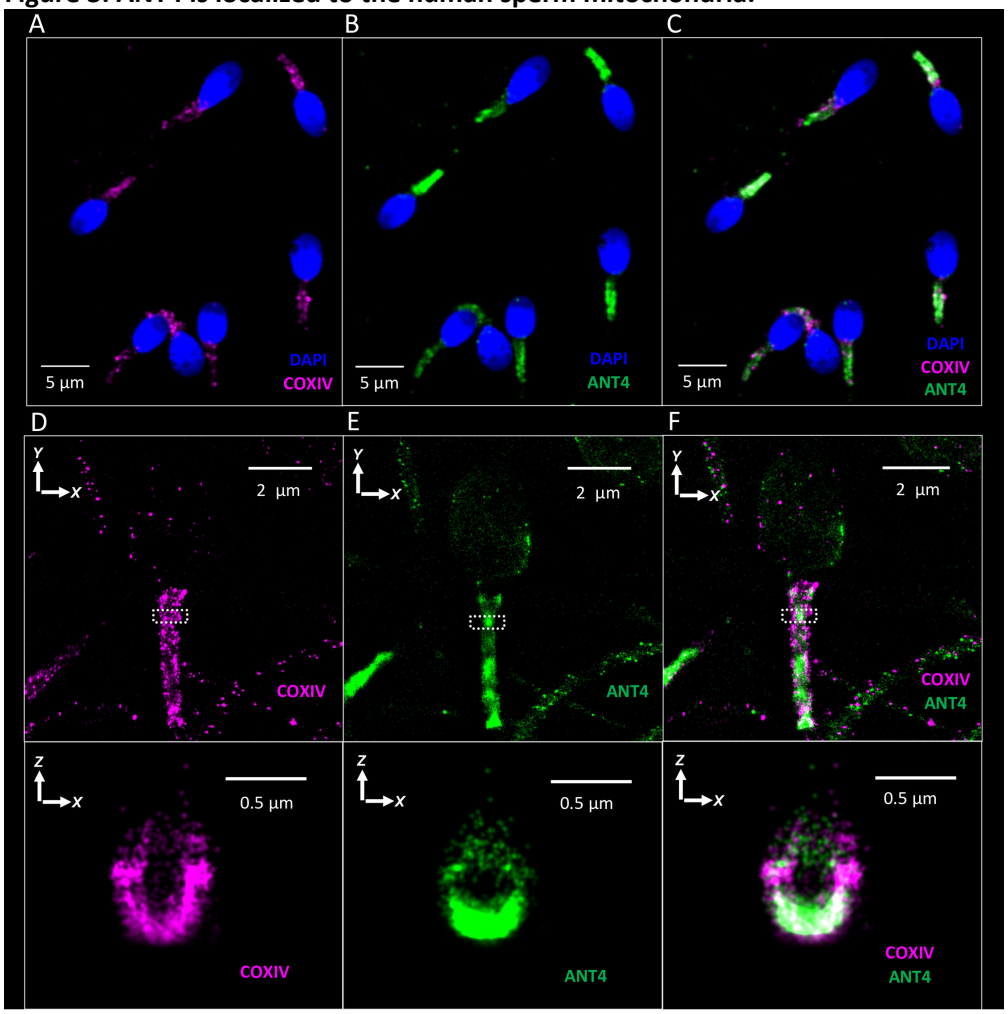

709

710 **Figure 4: Effects of small molecule uncouplers on human sperm ATP production and sperm**
711 **membrane proton current.**

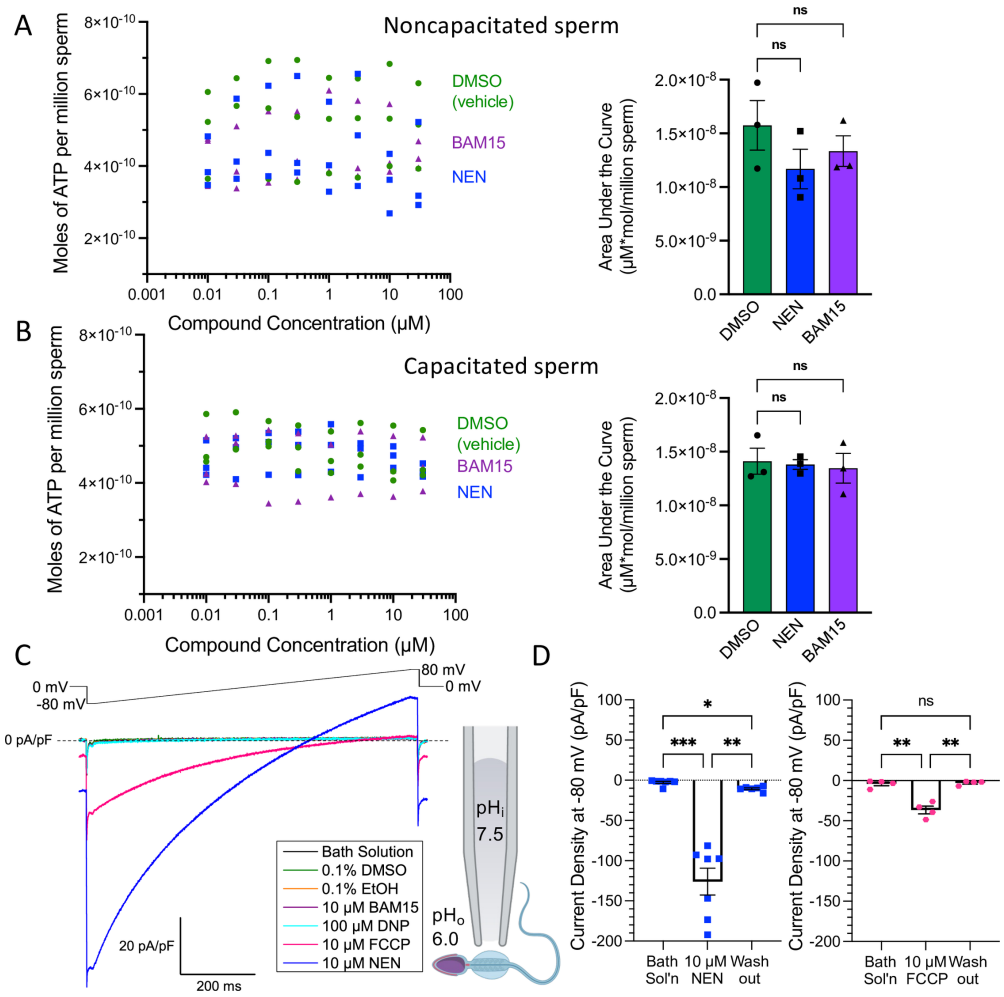

712

Supplementary Information for

Mitochondrial uncouplers impair human sperm motility without altering ATP content

Short Title: Mitochondrial uncouplers reduce human sperm motility but not ATP content

Will M. Skinner[1], Natalie T. Petersen[2,#3], Bret Unger[4], Shaogeng Tang[5,6], Emiliano Tabarsi[2,#7], Julianna Lamm[2,#8], Liza Jalalian[9], James Smith[10], Ambre M. Bertholet[11,#12], Ke Xu[4,13,14], Yuriy Kirichok[11], Polina V. Lishko[2,15,*].

[1] Endocrinology Graduate Group, University of California, Berkeley, Berkeley, California, United States of America

[2] Department of Molecular and Cell Biology, University of California, Berkeley, Berkeley, California, United States of America

[3] Department of Obstetrics and Gynecology, Stanford University School of Medicine, Palo Alto, California, United States of America

[4] Department of Chemistry, University of California, Berkeley, Berkeley, California, United States of America

[5] Department of Biochemistry, Stanford University School of Medicine, Stanford, California, United States of America

[6] Sarafan ChEM-H, Stanford University, Stanford, California, United States of America

[7] Keck School of Medicine, University of Southern California, Los Angeles, California, United States of America

[8] Dewpoint Therapeutics, Boston, Massachusetts, United States of America

[9] Department of Obstetrics and Gynecology, University of California, San Francisco Center for Reproductive Health, San Francisco, California, United States of America

[10] Department of Urology, University of California, San Francisco, San Francisco, California, United States of America

[11] Department of Physiology, University of California San Francisco, San Francisco, California, United States of America

[12] Department of Physiology, David Geffen School of Medicine, University of California Los Angeles, Los Angeles, California, United States of America

[13] California Institute for Quantitative Biosciences, University of California, Berkeley, California, United States of America

[14] Chan Zuckerberg Biohub, San Francisco, California, United States of America

[15] Center for Reproductive Longevity and Equality, Buck Institute for Research on Aging, Novato, California, United States of America

*Corresponding Author: Polina V. Lishko
Email: lishko@berkeley.edu

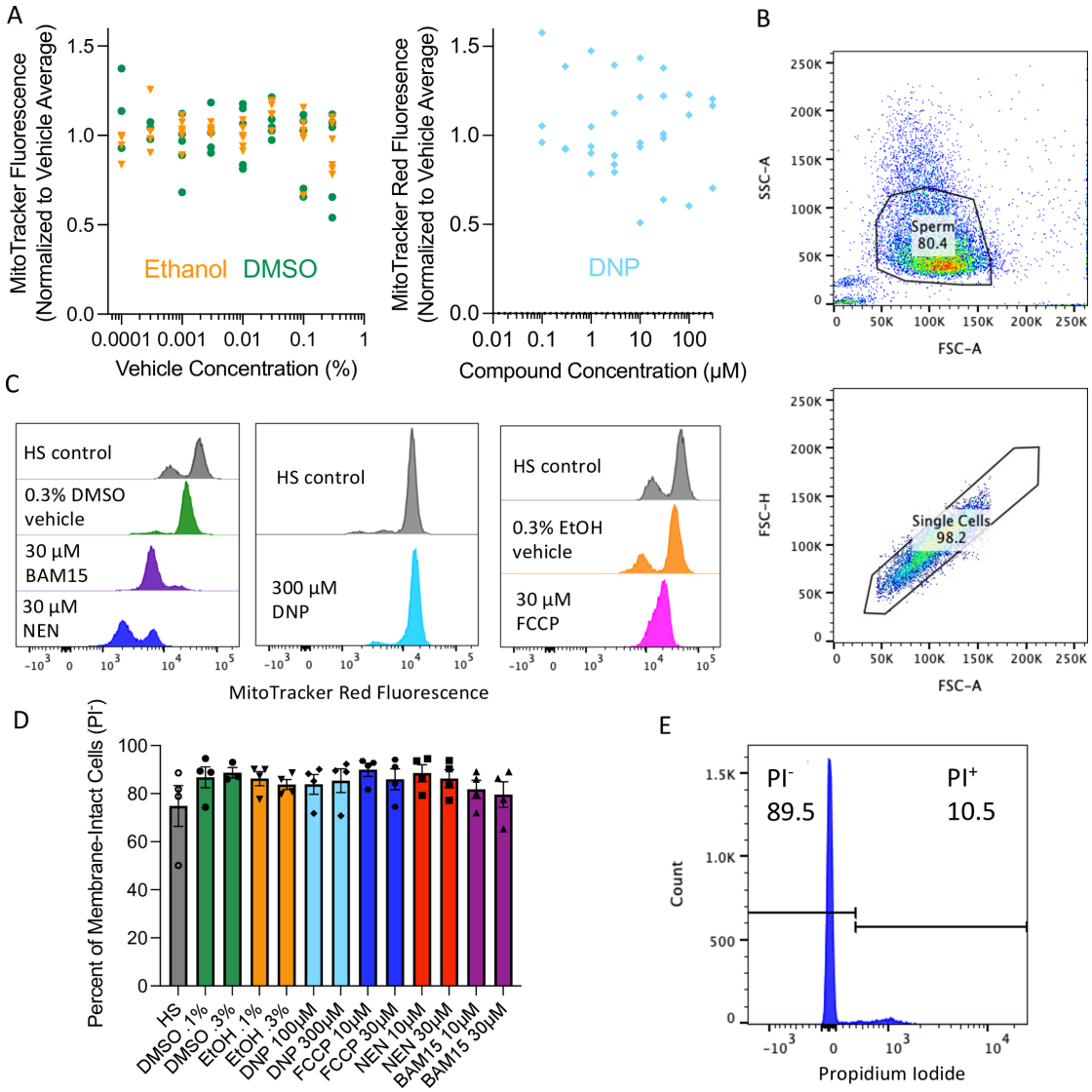

Figure S1. Validation of flow cytometric assessment of human sperm mitochondrial membrane potential A) Left: Effect of compound vehicles on MitoTracker fluorescence. **Right:** Effect of the uncoupler 2, 4, DNP on MitoTracker Fluorescence. In both, nonlinear regression performed, but not shown or reported because adjusted R^2 values were <.1. B) Representative gating logic for flow cytometry experiments, isolating individual sperm cells from debris (top) and aggregations (bottom). C) Representative flow cytometry histograms for MitoTracker Red CMX-Ros Mitochondrial Membrane Potential Assays. D) Percent of propidium iodide-excluding cells (membrane intact) after 30-minute incubation with compounds, as measured by flow cytometry. Each data point represents the average of 10,000 cells, and error bars represent SEM. All conditions were compared to DMSO .1% using Dunnett's Multiple Comparisons Test, and no

conditions were significantly different. E) Representative flow cytometry result of propidium iodide vitality assay.

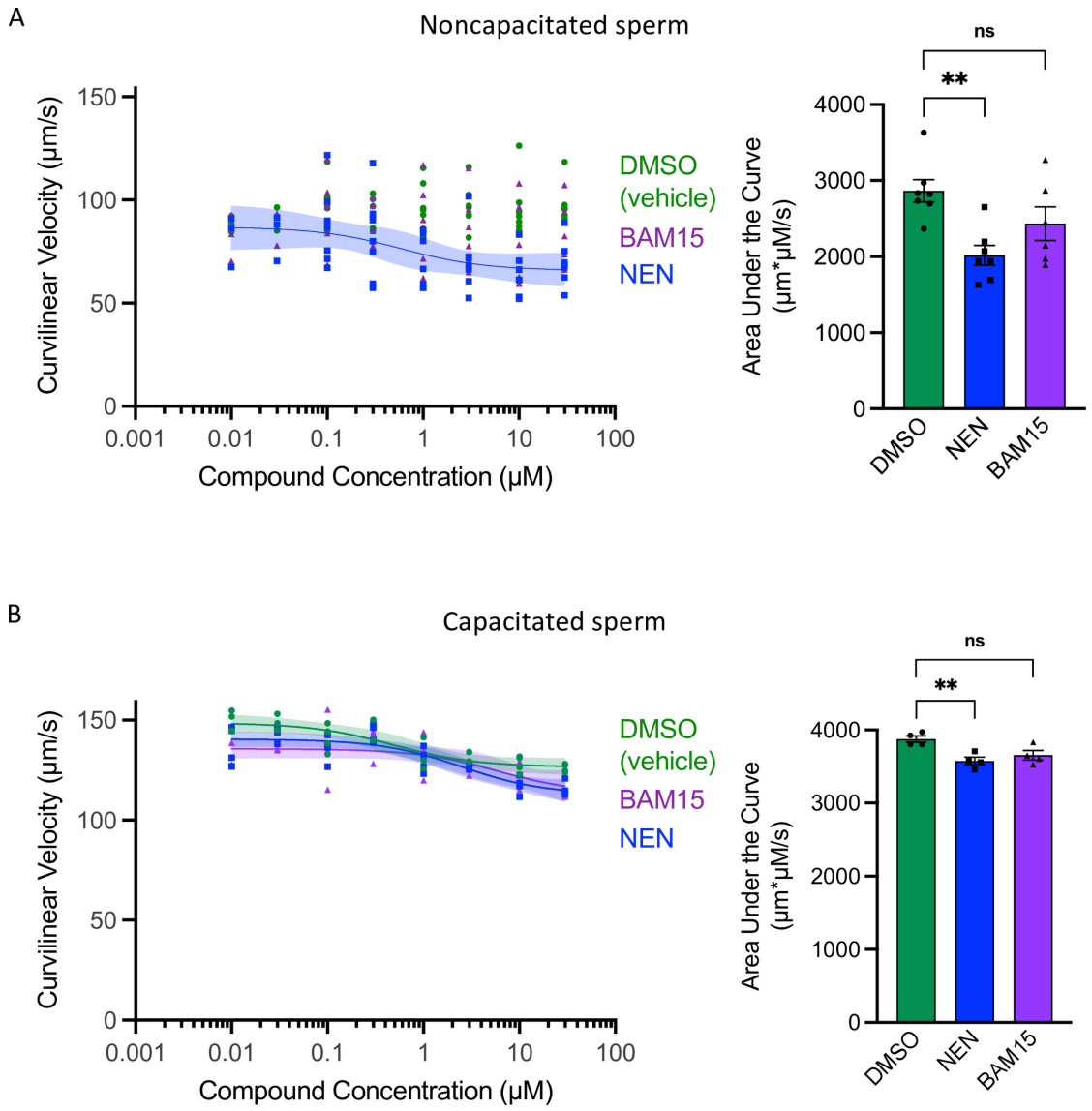

Figure S2: Effects of small molecule uncouplers on human sperm curvilinear velocity as measured by computer-aided sperm analysis. **A)** Curvilinear velocity analysis of noncapacitated human sperm cells. Left: Each data point represents the average curvilinear velocity of at least 200 sperm cells. Nonlinear least squares regression performed using an unweighted [inhibitor] vs. response three parameter model (Hill Slope = -1.0), identifying "unstable" fits. Shaded areas indicate 95% confidence bands for true location of each nonlinear fit curve. The nonlinear regression fit for NEN had an Adjusted R^2 value of 0.1833. BAM15 & DMSO nonlinear regressions not shown because their adjusted R^2 values were below 0.1. NEN IC_{50} Asymmetrical 95% CI interval: 0.07433 µM to 6.950 µM. Outliers tested using a ROUT coefficient of 1%, with two outliers in the DMSO condition excluded. NEN residuals passed the Replicates and homoscedasticity tests, but failed the D'Agostino-Pearson omnibus normality test with a p-value of .0366. Right: Area Under the Curve analysis for data at left. Each data point represents the area under the curve of one biological replicate. **B)** Curvilinear Velocity analysis of

capacitated human sperm cells. Left: Nonlinear Regression performed as in A. The nonlinear regression fit for DMSO had an Adjusted R^2 value of 0.7328 with an IC_{50} 95% Confidence Interval of 0.1126 µM to 1.925 µM. The nonlinear regression fit for NEN had an Adjusted R^2 value of 0.7275 with an IC_{50} 95% Confidence Interval of 0.9469 µM to 7.230 µM. The nonlinear regression fit for BAM15 had an Adjusted R^2 value of 0.3885 with an IC_{50} 95% Confidence Interval of 0.8117 µM to 294309381 µM. All tests performed as in A, with no outliers detected, and with residuals passing all tests, except that the residuals for NEN failed the test for homoscedasticity with a P-value of .006. Right: Area Under the Curve analysis for data at left.

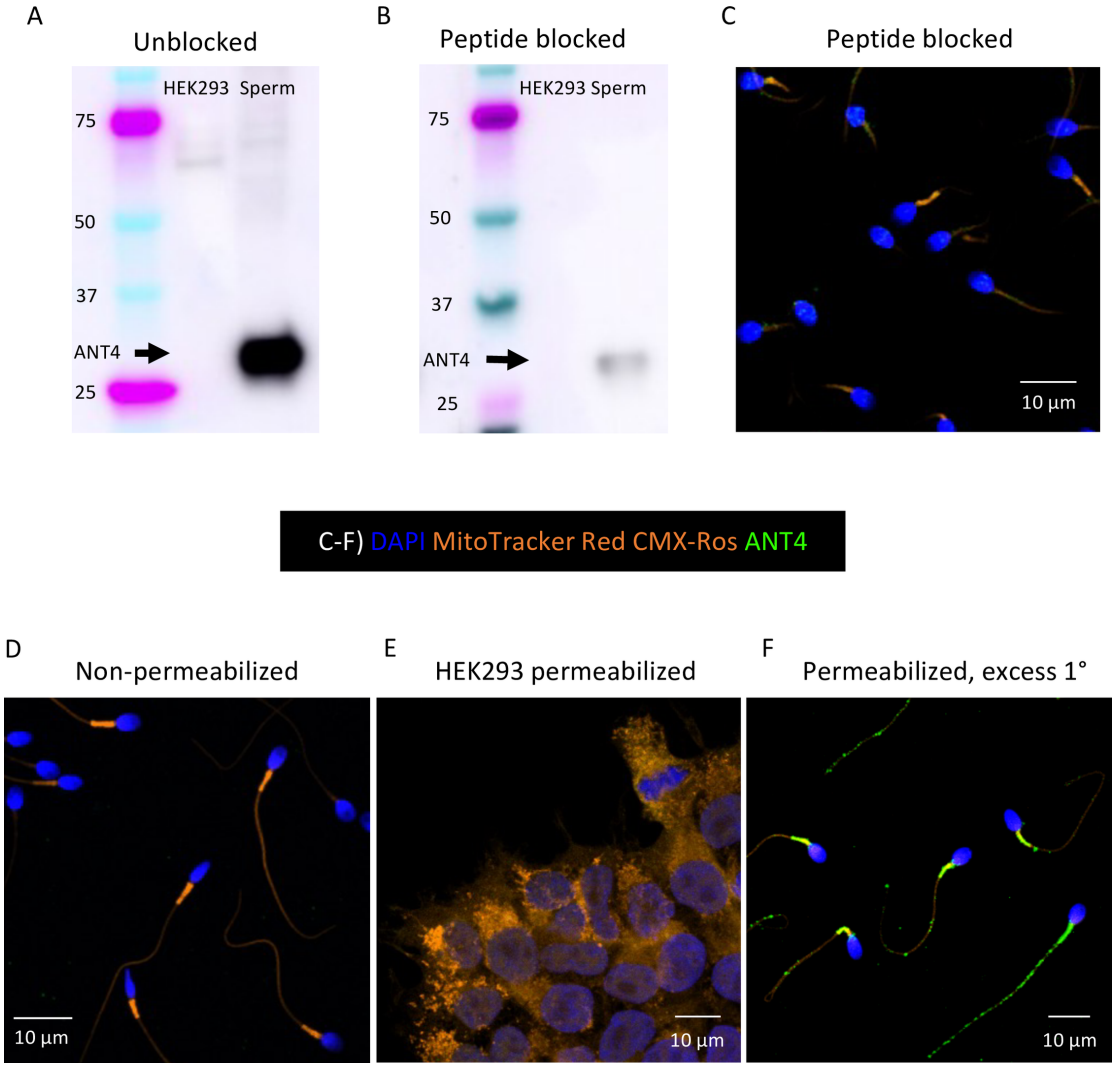

Figure S3: Human ANT4 polyclonal antibody validation. A,B) hANT4 Western blot of HEK293 cells and human sperm. A), unblocked; B) blocked with immunizing peptide. C) ICC of permeabilized human sperm incubated with hANT4 pAb preblocked with immunizing peptide and 50 nM Mitotracker Red CMX-Ros. **D)** ICC of non-permeabilized human sperm labelled as in C. E) ICC of permeabilized HEK293 cells labelled as in C. F) Permeabilized human sperm cells incubated with excess hANT4 pAb primary antibody (.4 µg/mL) and 50 nM MitoTracker Red CMX-Ros. In C-F, Orange – MitoTracker Red CMX-Ros, Blue – Dapi, Green – hANT4. All images are maximum intensity projections of sequential confocal image z-slices.

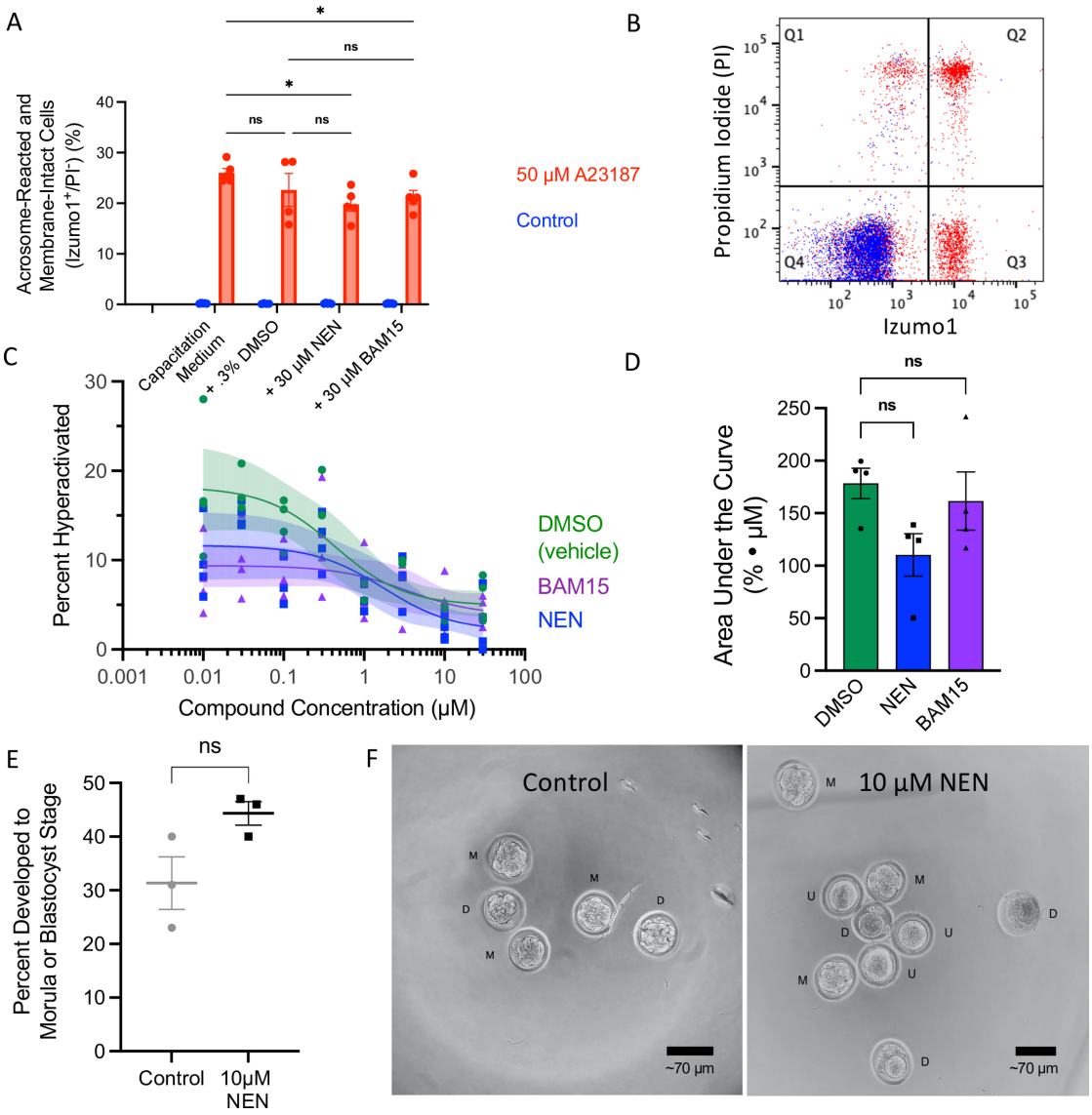

Figure S4: NEN and BAM15 have no effect on human sperm acrosome reaction competence or human sperm hyperactivated motility, and NEN has no effect on Mouse IVF success A) Percentage of unfixed, capacitated human sperm cells that were acrosome-reacted and membrane-intact (Izumo1$^+$/Propidium Iodide$^-$) as measured by flow cytometry, after incubation with and without the calcium ionophore A23187. Each data point represents the percentage of 100,000 cells showing this fluorescence pattern. Error bars represent SEM, and significance was calculated by Tukey's multiple comparisons test, with individual variances computed for each comparison. All combinations were compared, but for clarity, not all comparisons are shown. All non-shown comparisons were not significant. **B)** Representative data plots from one run of flow cytometry, comparing ionophore A23187-treated (red) and control cells (blue). **C)** Representative confocal microscopy image of A23187-treated sperm cells taken from flow cytometry run, showing Izumo1 staining in red, and DAPI staining in blue. AR: Acrosome Reacted, AI: Acrosome Intact. **D)** Percent of capacitated human sperm cells

displaying hyperactivated motility, as measured by computer-aided sperm analysis. Each data point represents the percent of at least 200 sperm cells showing hyperactivated motility. Nonlinear least squares regression performed using an unweighted [inhibitor] vs. response three parameter model (Hill Slope = -1.0), identifying "unstable" fits. Shaded areas indicate 95% confidence bands for true location of each nonlinear fit curve. The nonlinear regression fit for DMSO had an Adjusted R^2 value of 0.6501, and an IC_{50} 95% CI of 0.1052 µM to 2.131 µM. The nonlinear regression fit for NEN had an Adjusted R^2 value of 0.5062, and an IC_{50} 95% CI of 0.2957 µM to 12.04 µM. The nonlinear regression fit for BAM15 had an Adjusted R^2 value of 0.1667, and an IC_{50} 95% CI of 0.1418 µM to +infinity. **E)** Area under the curve analysis of hyperactivation data from panel E. Each data point represents the area under the curve of one biological replicate, error bars represent SEM, and statistical significance calculated using Dunnett's Multiple Comparisons Test. **F)** Quantification of mouse eggs that developed to morula or blastocyst stage after *In vitro* fertilization (IVF) using SMU-treated sperm. Significance calculated using a one-tailed ratio paired t-test. **G)** Representative micrographs of mouse embryos 3.5 days after IVF. Left, oocytes exposed to control sperm; Right, oocytes exposed to 10 µM NEN-treated sperm. M - Morula, D - Dead, U - Unfertilized.

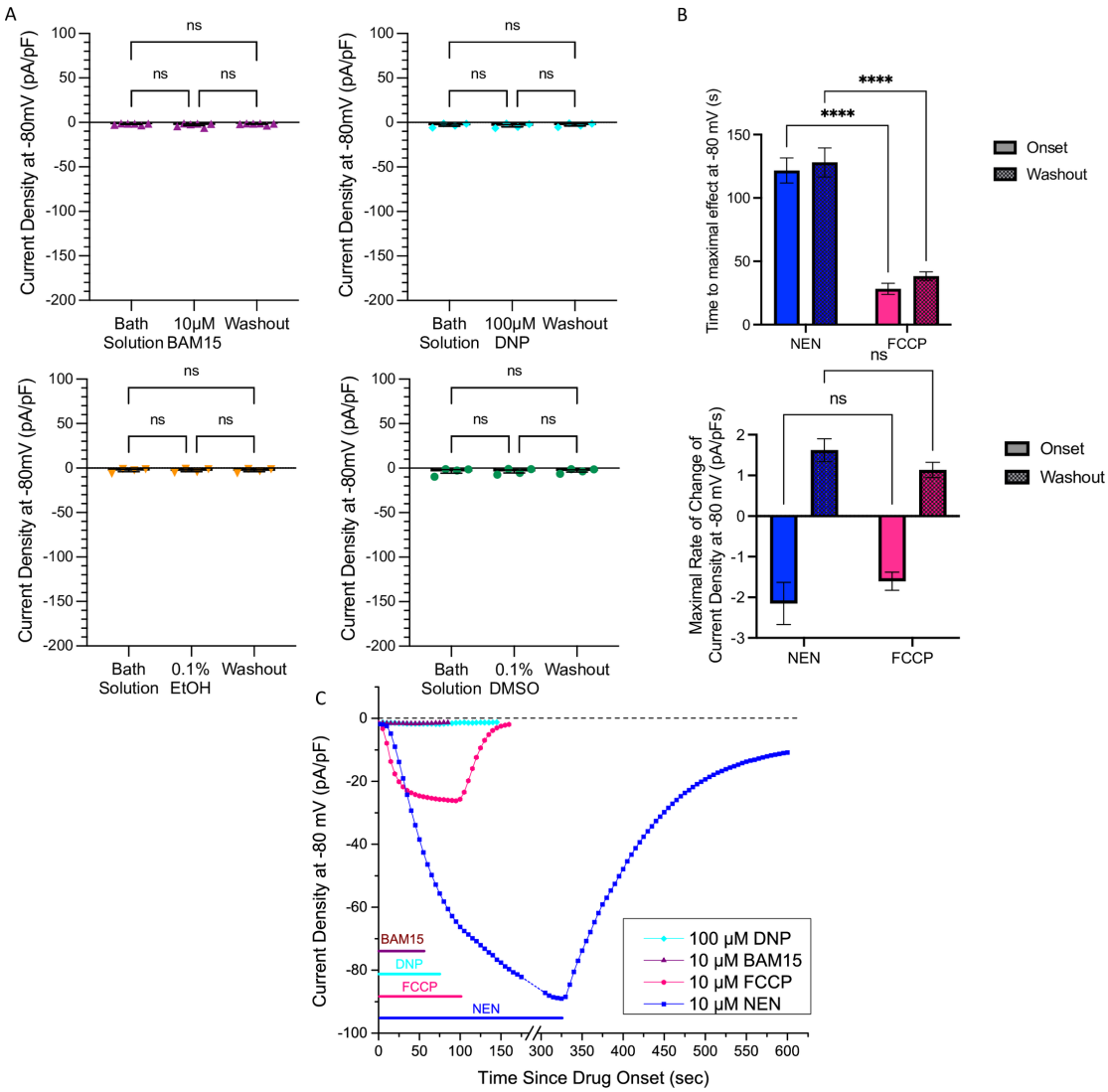

Figure S5: Supplemental electrophysiology quantifications. A) 10 µM BAM15, 100 µM DNP, 0.1% EtOH**,** and 0.1% DMSO have no effect on sperm plasma membrane current densities. Significance calculated using Tukey's multiple comparisons test. **B)** NEN takes longer to reach maximal uncoupling than FCCP (top), but their maximum rates of current density increase are similar (bottom). Significance calculated using Šídák's multiple comparison's test, with a single pooled variance **C)** Time courses of current density at -80 mV during application of compounds. Colored bars represent time period during which each compound was being applied. Dotted line in NEN time course represents a period where other electrophysiological tests were performed on that cell.